Journal of Applied Physics

A comparison of magnetoconductivities between type-I and type-II Weyl semimetals

Cite as: J. Appl. Phys. **129**, 125104 (2021); https://doi.org/10.1063/5.0039554
Submitted: 04 December 2020 . Accepted: 07 March 2021 . Published Online: 25 March 2021

K. Morishima, and K. Kondo

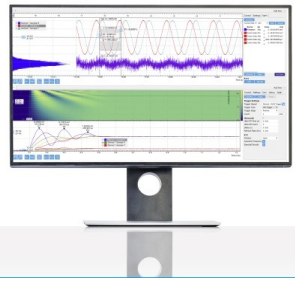

AIP Publishing

Journal of Applied Physics ARTICLE scitation.org/journal/jap

A comparison of magnetoconductivities between type-I and type-II Weyl semimetals

Cite as: J. Appl. Phys. **129**, 125104 (2021); doi: 10.1063/5.0039554
Submitted: 4 December 2020 · Accepted: 7 March 2021 ·
Published Online: 25 March 2021

K. Morishima and K. Kondo[a)]

AFFILIATIONS

Research Institute for Electronic Science, Hokkaido University, Kita-ku, Kita-20, Nishi-10, Sapporo, Hokkaido, Japan

[a)]**Author to whom correspondence should be addressed:** kkondo@es.hokudai.ac.jp. **URL:** http://qed4.es.hokudai.ac.jp/kondo.htm

ABSTRACT

It is well known that Weyl semimetals (WSMs) are classified into two types of type-I and type-II depending on whether or not they have electron and hole pockets. Also, these WSMs have peculiar transport properties such as negative longitudinal magnetoresistance and planar Hall effect because of a chiral anomaly. In this paper, however, we show that the chiral anomaly can cause positive longitudinal magnetoresistance in type-II WSMs. Here, we investigate longitudinal and transverse magnetoconductivities of time reversal symmetry broken type-I and type-II WSMs using a tight-binding model. The model allows us to describe both types of type-I and type-II WSMs by tuning parameters, and it has two Weyl points that are separated along the k_x-direction. The numerical calculations of these conductivities are performed using the Boltzmann equation including the Berry curvature. It is found that longitudinal magnetoconductivities in the x-direction can have both positive and negative values depending on the magnitude of the inclination of a Weyl cone. This is because the zeroth Landau energy-level becomes either a hole-like one or an electron-like one depending on the magnitude of the inclination of the Weyl cone in type-II WSMs. These results imply that we can make a high MR-ratio device using type-II WSMs by tuning the inclination of their cones if it is possible to change their energy bands by the application of electric field and so on.

I. INTRODUCTION

Many researchers have paid much attention to topological materials from the viewpoint of fundamental physics[1–3] and the application to spintronics devices.[4–7] Recently, many kinds of topological materials are proposed theoretically and found experimentally. Weyl semimetals (WSMs) are one kind of topological materials among them. WSMs are characterized by some pairs of Weyl points with opposite chirality. In the momentum space, each Weyl point can be regarded as a monopole and an antimonopole of the Berry curvature. WSMs have linear energy dispersions near Weyl points, which are called the Weyl cone. Weyl semimetals (WSMs) are classified into two types of type-I and type-II[8] depending on whether or not they have electron and hole pockets. In both types of WSMs, they exhibit a characteristic electronic structure and quantum anomaly. They are called "Fermi arc" and "chiral anomaly,"[9] respectively. The Fermi arc is an electronic state emerging on the surfaces of WSMs and connects the points where two Weyl points are projected to the surface. Therefore, Fermi arcs are tangent to the bulk Fermi surface projections. The 2D quantum Hall planes perpendicular to the direction of Weyl point separation have nonzero Berry flux through them and act like a Chern insulator between these Weyl points. As a result, the Fermi arc is regarded as the chiral edge state of the Chern insulator. This feature can be used to detect WSMs using angle-resolved photoemission spectroscopy (ARPES). In recent years, it is reported that TaAs, TaP, NbAs, and NbP[10–14] are type-I WSMs and WTe_2, $MoTe_2$, and $YbMnBi_2$[15–17] are type-II WSMs. A chiral anomaly is a quantum anomaly where the net chirality in the system does not conserve. In the presence of an electric and a magnetic field, the chiral current flows between two Weyl points due to the chiral anomaly. It is known that the difference between the chiral chemical potentials of two Weyl cones by a chiral anomaly causes the chiral magnetic effect.[18,19] Since the current by the chiral magnetic effect flows, the negative longitudinal magnetoresistance occurs. The negative longitudinal magnetoresistance has been observed in NbP, TaP, and NbAs.[13–15,20,21] Moreover, in WSMs, the planar Hall effect also occurs and has been observed in GdPtBi and TaP.[22,23] Many researchers have reported that the chiral anomaly in WSMs causes the negative longitudinal magnetoresistance. However, we have found that the positive longitudinal magnetoresistance can also occur depending on the tilt of the Weyl cone.

In this study, we investigate the electronic structures of time reversal symmetry (TRS) broken type-I and type-II WSMs. Moreover, we investigate longitudinal and transverse magnetoconductivities of them and discuss the origin of the positive longitudinal magnetoresistance.

II. THEORY

A. TRS broken WSM model

In this paper, we utilize the following TRS broken Hamiltonian:[24]

$$\begin{aligned} H(\boldsymbol{k}) = &-[2m - t'(\cos k_y + \cos k_z) \\ &- 2t_x(\cos k_x - \cos k_0)]\sigma_x \\ &- 2t \sin k_y \sigma_y - 2t \sin k_z \sigma_z + \gamma(\cos k_x - \cos k_0)\sigma_0, \end{aligned} \tag{1}$$

where σ_i are the Pauli matrices. This Hamiltonian has two Weyl points at $\boldsymbol{k} = (\pm k_0, 0, 0)$ and k_0 is set to $\pi/2$ for simplicity. It does not lose generality. This Hamiltonian allows us to describe both types of type-I and type-II WSMs by tuning parameters γ. γ is the parameter that determines the inclination of the Weyl cone. In this model, Weyl cone can be tilted in the k_x-direction. When $|\gamma|$ is less than $2t$, this model becomes to describe type-I WSMs. On the other hand, when $|\gamma|$ is more than $2t$, it becomes to describe type-II WSMs. Since we investigate the magnetoconductivities of WSMs in this paper, we need to calculate their electronic structures under the magnetic field. Here, we consider the case where the magnetic field of $\boldsymbol{B} = (B, 0, 0)$ is applied along the x-direction. In this case, we can replace the wave vector of $\boldsymbol{k}$ in Eq. (1) by taking the Landau gauge condition of $\boldsymbol{A} = (0, 0, yB)$ as follows:

$$\boldsymbol{k} = \left(k_x, k_y, k_z + \frac{eBy}{\hbar}\right). \tag{2}$$

Then, the Hamiltonian under the magnetic field is given by

$$\begin{aligned} H(\boldsymbol{k}) = &-\left[2m - t'\left(2 - \frac{k_y{}^2}{2} - \frac{(k_z + \frac{eBy}{\hbar})^2}{2}\right)\right. \\ &\left. - 2t_x\left(1 - \frac{k_x{}^2}{2} - \cos k_0\right)\right]\sigma_x - 2tk_y\sigma_y \\ &- 2t\left(k_z + \frac{eBy}{\hbar}\right)\sigma_z + \gamma\left(1 - \frac{k_x{}^2}{2} - \cos k_0\right)\sigma_0. \end{aligned} \tag{3}$$

Here, we use the long wavelength approximation. We introduce the following creation and annihilation operators:[25,26]

$$\begin{aligned} a &\equiv -[(y + l_B{}^2 k_z)/l_B + l_B \partial_y]/\sqrt{2}, \\ a^\dagger &\equiv -[(y - l_B^2 k_z)/l_B - l_B \partial_y]/\sqrt{2}, \end{aligned}$$

where the magnetic length $l_B = \sqrt{\hbar/eB}$. To derive Landau energy-levels, we need to rewrite Eq. (3) using a and $a^\dagger$. This problem can be solved using the following unitary matrix:

$$U = \frac{1}{\sqrt{2}}\begin{bmatrix} 1 & 1 \\ 1 & -1 \end{bmatrix}.$$

As a result, the Hamiltonian can be rewritten as follows:

$$\tilde{H} = U^\dagger H U = \begin{bmatrix} M_1 + M_2 & \eta a \\ \eta a^\dagger & -M_1 + M_2 \end{bmatrix}, \tag{4}$$

where

$$\begin{aligned} M_1 &= 2t_x(1 - k_x^2/2 - \cos k_0) + 2(t' - m) - \omega(a^\dagger a + 1/2), \\ M_2 &= \gamma(1 - k_x^2/2 - \cos k_0), \omega = t'/l_B^2, \eta = 2\sqrt{2}t/l_B. \end{aligned}$$

We assume that the eigenvectors of this Hamiltonian are $\phi_n = (a_n|n-1\rangle, b_n|n\rangle)^{\mathrm{T}}$, where n is the index of the Landau energy-level and a_n, b_n are the normalization factors. When n is equal to zero, the eigenvector is $\phi_0 = (0, |0\rangle)^{\mathrm{T}}$. Then, the Schrödinger equation $H\phi_n = E\phi_n$ becomes the following one in a matrix form:

$$\det\begin{bmatrix} M_{n-1} + M_2 - E & \eta\sqrt{n} \\ \eta\sqrt{n} & -M_n + M_2 - E \end{bmatrix} = 0, \tag{5}$$

where E is the eigenvalue and $M_n = 2t_x(1 - k_x^2/2 - \cos k_0) + 2(t' - m) - \omega(n + 1/2)$. The following Landau energy-levels can be obtained by solving Eq. (5):

$$\begin{aligned} E_0 = &\gamma\left(1 - \frac{k_x^2}{2} - \cos k_0\right) + \frac{t'}{2l_B^2} \\ &- 2t_x\left(1 - \frac{k_x^2}{2} - \cos k_0\right) - 2(t' - m), \end{aligned} \tag{6}$$

$$\begin{aligned} E_n^\pm = &\gamma\left(1 - \frac{k_x^2}{2} - \cos k_0\right) + \frac{t'}{2l_B^2} \\ &\pm \sqrt{[2t_x\left(1 - \frac{k_x^2}{2} - \cos k_0\right) + 2(t' - m) - \frac{nt'}{2l_B^2}]^2 + \frac{8t^2}{l_B^2}n}. \end{aligned} \tag{7}$$

B. Formulation of magnetoconductivity

To investigate longitudinal and transverse magnetoconductivities, we perform numerical calculations of magnetoconductivities using the Boltzmann equation including the Berry curvature. In the presence of the Berry curvature, the equations of motion for a charged particle are given by

$$\dot{\boldsymbol{r}} = \boldsymbol{v}_{\boldsymbol{k}} - \dot{\boldsymbol{k}} \times \boldsymbol{\Omega}_{\boldsymbol{k}}, \tag{8}$$

$$\hbar\dot{\boldsymbol{k}} = -e\boldsymbol{E} - e\dot{\boldsymbol{r}} \times \boldsymbol{B}, \tag{9}$$

where $\boldsymbol{v}_{\boldsymbol{k}}$ is the group velocity of a charged particle and $\boldsymbol{\Omega}_{\boldsymbol{k}}$ is the

Berry curvature. From Eqs. (8) and (9), we can obtain[27]

$$\dot{\boldsymbol{r}} = D_{\boldsymbol{k}}\left[\boldsymbol{v}_{\boldsymbol{k}} + \frac{e}{\hbar}(\boldsymbol{E}\times\boldsymbol{\Omega}_{\boldsymbol{k}}) + \frac{e}{\hbar}(\boldsymbol{v}_{\boldsymbol{k}}\cdot\boldsymbol{\Omega}_{\boldsymbol{k}})\boldsymbol{B}\right], \tag{10}$$

$$\hbar\dot{\boldsymbol{k}} = D_{\boldsymbol{k}}\left[-e\boldsymbol{E} - e(\boldsymbol{v}_{\boldsymbol{k}}\times\boldsymbol{B}) - \frac{e^2}{\hbar}(\boldsymbol{E}\cdot\boldsymbol{B})\boldsymbol{\Omega}_{\boldsymbol{k}}\right], \tag{11}$$

where $D_{\boldsymbol{k}}$ is defined by $[1 + e(\boldsymbol{B}\cdot\boldsymbol{\Omega}_{\boldsymbol{k}})/\hbar]^{-1}$. Substituting Eqs. (10) and (11) to the Boltzmann equation, the magnetoconductivity can be obtained as follows:[28]

$$\sigma_{ij} = e^2\tau\int_{BZ}\frac{d^3\boldsymbol{k}}{(2\pi)^3}D_{\boldsymbol{k}}\left(v_i + \frac{eB_i}{\hbar}(\boldsymbol{v}_{\boldsymbol{k}}\cdot\boldsymbol{\Omega}_{\boldsymbol{k}})\right) \times\left(v_j + \frac{eB_j}{\hbar}(\boldsymbol{v}_{\boldsymbol{k}}\cdot\boldsymbol{\Omega}_{\boldsymbol{k}})\right)\left(-\frac{\partial f(\epsilon_{\boldsymbol{k}})}{\partial\epsilon_{\boldsymbol{k}}}\right), \tag{12}$$

where τ is the relaxation time and $f(\epsilon_{\boldsymbol{k}})$ is the Fermi–Dirac distribution function. Here, the current flows in the i-direction and an electric field is applied along the j-direction.

III. RESULTS AND DISCUSSION

First, we show the numerical calculation results of electronic structures of type-I and type-II WSMs, respectively. In the case of type-I WSMs, we set the parameters $t_x = t$, $t' = m = 2t$, and $\gamma = 0$. On the other hand, in the cases of type-II WSMs, we set the parameters $t_x = t$, $t' = m = 2t$, and $\gamma = \pm 2.5t$. We show the electronic structures of type-I WSMs and type-II WSMs in Fig. 1, respectively. Henceforth, we call type-II WSMs with $\gamma = -2.5$ ($\gamma = 2.5$) as A-type-II WSMs (B-type-II WSMs). The A-type-II WSMs have a pair of Weyl cones titled toward each other as shown in Fig. 1(b). On the other hand, the B-type-II WSMs have a pair of Weyl cone tilted away from each other as shown in Fig. 1(c).[29] In all the cases of type-I, A-type-II, and B-type-II WSMs, the value of chirality χ at $\boldsymbol{k} = (k_0, 0, 0)$ is equal to -1 and that at $\boldsymbol{k} = (-k_0, 0, 0)$ is equal to $+1$.

When the magnetic field is applied along the x-direction, Landau energy-levels of type-I, A-type-II, and B-type-II WSMs are shown in Fig. 2. These figures are the cross-sectional views of energy structures along the path connecting Weyl points. Here, we are applying a strong magnetic field of $B = 50$ T in order to emphasize these Landau energy-levels. The red lines indicate the zeroth Landau energy-levels. The zeroth Landau energy-levels of type-I WSMs have a valley at the origin with the magnetic field applied in the positive direction of the x-axis as shown in Fig. 2(a). There exist the electron-like zeroth Landau energy-levels. Specifically, they have positive effective mass. However, when the magnetic field is applied in the negative direction of the x-axis, the zeroth Landau energy-levels has a peak at the origin as shown in Fig. 2(d). There exist the hole-like zeroth Landau energy-levels. Namely, they have negative effective mass. These results indicate that in type-I WSMs, reversing the direction of the magnetic field gets the effective mass of the zeroth Landau energy-levels to be changed from positive to negative. On the other hand, Figs. 2(b), 2(c), 2(e), and 2(f) show that A-type-II (B-type-II) WSMs have the electron-like (the hole-like) zeroth Landau energy-levels with applying the magnetic field even in either direction of the x-axis. Specifically, the zeroth Landau energy-levels of A-type-II (B-type-II) WSMs have the positive (the negative) effective mass, regardless of the direction of the magnetic field. On the other hand, Fig. 3 shows Landau energy-levels of type-I, A-type-II, and B-type-II WSMs under the magnetic field of $B = 50$ T applied perpendicular to the direction (y-axis) of Weyl point separation. The red lines indicate the zeroth Landau energy-level of the Weyl cone having $\chi = +1$, and the blue lines indicate the zeroth Landau energy-level of the Weyl cone having $\chi = -1$. We find that in all the cases of type-I, A-type-II, and B-type-II WSMs, the Weyl cone having $\chi = +1$ ($\chi = -1$) has the zeroth Landau energy-level with the negative (the positive) gradient under the magnetic field applied in the positive direction of the y-axis as shown in Fig. 3(a). In contrast, we find that in all the cases of type-I, A-type-II, and B-type-II

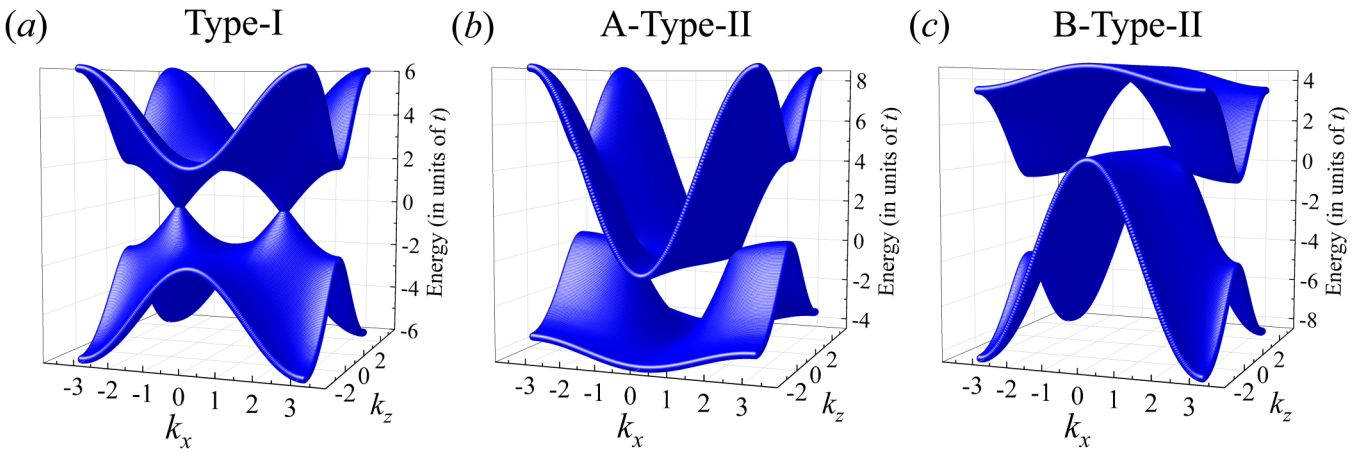

FIG. 1. The electronic structures of (a) type-I WSMs ($\gamma = 0$), (b) A-type-II WSMs ($\gamma = -2.5t$), and (c) B-type-II WSMs ($\gamma = 2.5t$). We set the parameters $t_x = t$, $t' = m = 2t$, and $k_y = 0$.

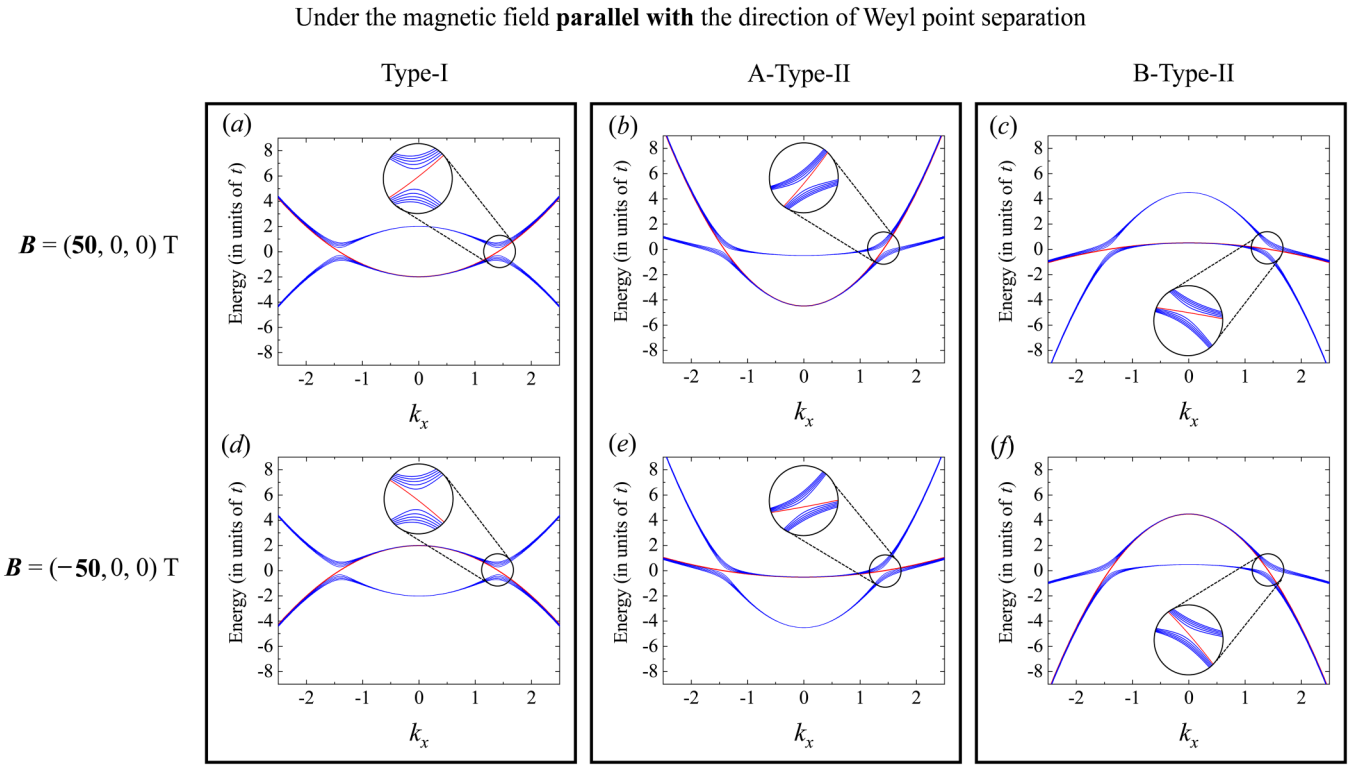

FIG. 2. Landau energy-levels of (a) type-I WSMs ($\gamma = 0$), (b) A-type-II WSMs ($\gamma = -2.5t$), and (c) B-type-II WSMs ($\gamma = 2.5t$) under the magnetic field of $\boldsymbol{B} = (50, 0, 0)$ T. Landau energy-levels of (d) type-I WSMs ($\gamma = 0$), (e) A-type-II WSMs ($\gamma = -2.5t$), and (f) B-type-II WSMs ($\gamma = 2.5t$) under the magnetic field of $\boldsymbol{B} = (-50, 0, 0)$ T. The red line indicates the zeroth Landau energy-level.

WSMs, the Weyl cone having $\chi = +1$ ($\chi = -1$) has the zeroth Landau energy-level with the positive (the negative) gradient under the magnetic field applied in the negative direction of the y-axis as shown in Fig. 3(b).

Next, we show the numerical results of magnetoconductivities. Note that we have to calculate the magnetoconductivities in both the plane (the xy-plane) including the direction where Weyl points are separated and the other plane (the yz-plane) without including that in order to investigate the influence of chiral anomaly originating from Weyl points. Also, we perform the numerical calculations of the magnetoconductivities under the external magnetic field of 3 T throughout the paper. First, we show the numerical results of the magnetoconductivities in the xy-plane including the direction where Weyl points are separated. Figure 4 shows the longitudinal magnetoconductivities σ_{xx} under the magnetic field of $\boldsymbol{B} = (B_x, B_y, B_z) = (3\cos\theta, 3\sin\theta, 0)$ T in the xy-plane. Here, θ is the angle between the x-axis and the external magnetic field. The black lines, blue lines, and red lines show the longitudinal magnetoconductivities of type-I, A-type-II, and B-type-II WSMs, respectively. The solid curves represent the positive values, and the dotted curves represent the negative values. As shown in Fig. 4(a), it is found that the longitudinal magnetoconductivities (magnetoresistances) increase (decrease) as the direction of the magnetic field becomes more aligned to that of the electric field in both type-I and A-type-II WSMs. This phenomenon is well known and caused by the chiral anomaly and the chiral magnetic effect. However, it is found that the longitudinal magnetoconductivities (magnetoresistances) of B-type-II WSMs decrease (increase) as the direction of the magnetic field becomes more aligned to that of the electric field. Although the chiral anomaly also exists in B-type-II WSMs, the opposite phenomenon is occurring concerning the magnetoconductivity. We consider the reason why the opposite phenomenon occurs.

First, we consider the longitudinal magnetoconductivities under the magnetic field applied in the positive direction of the x-axis. In both type-I and A-type-II WSMs having the electron-like zeroth Landau energy-levels, under both the electric and magnetic fields applied in the positive direction of the x-axis, the electron carrier at the right Weyl cone sinks into the bulk to the negative direction of the x-axis, on the other hand, the electron carrier at the left Weyl cone moves up from the bulk to the negative direction of the x-axis. As a result, the chiral chemical potential of the left Weyl cone is higher than that of the right Weyl cone. However, in the B-type-II WSMs having the hole-like zeroth Landau energy-levels, under both the electric and the magnetic field applied in the positive direction of the x-axis, the electron carrier at the right Weyl cone moves up from the bulk to the negative direction of the

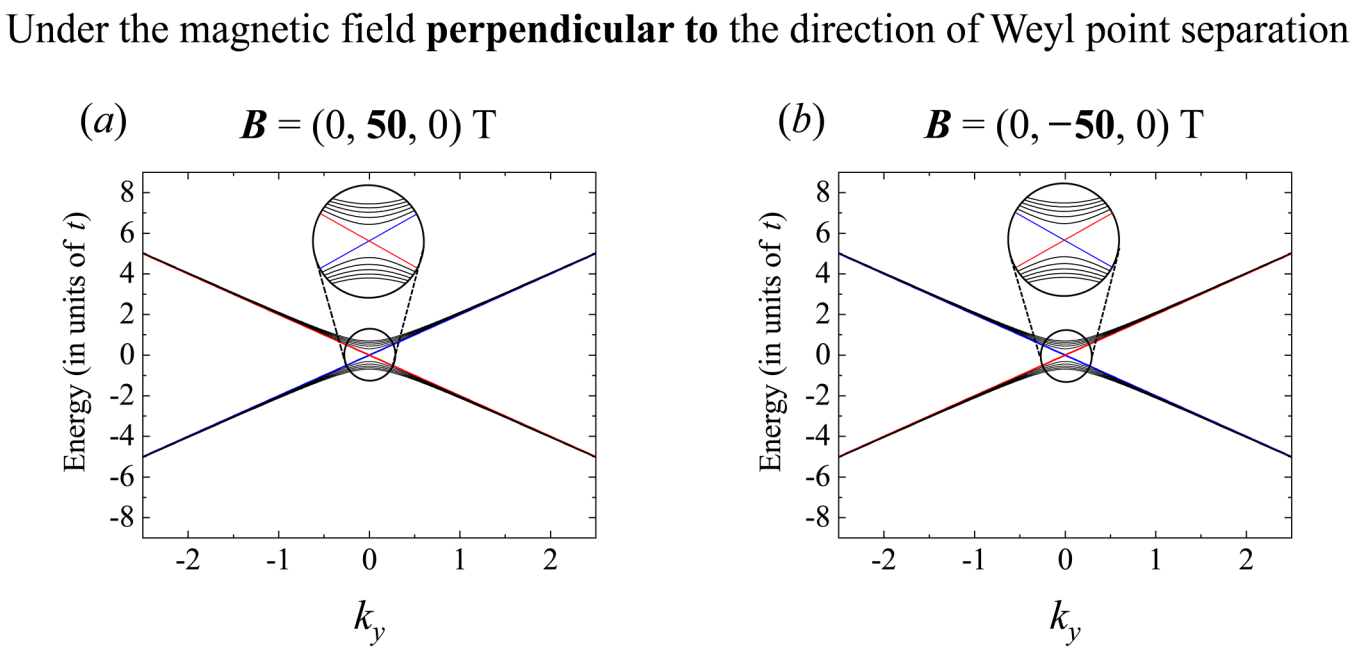

FIG. 3. (a) Landau energy-levels under the magnetic field of $\boldsymbol{B} = (0, 50, 0)$ T and (b) Landau energy-levels under the magnetic field of $\boldsymbol{B} = (0, -50, 0)$ T for all type-I, A-type-II, and B-type-II WSMs. All the parameters are the same as in Fig. 2. The red lines indicate the zeroth Landau energy-level of Weyl cone having $\chi = +1$, and the blue lines indicate the zeroth Landau energy-level of the Weyl cone having $\chi = -1$. The red and blue lines exchange depending on the direction of the magnetic field.

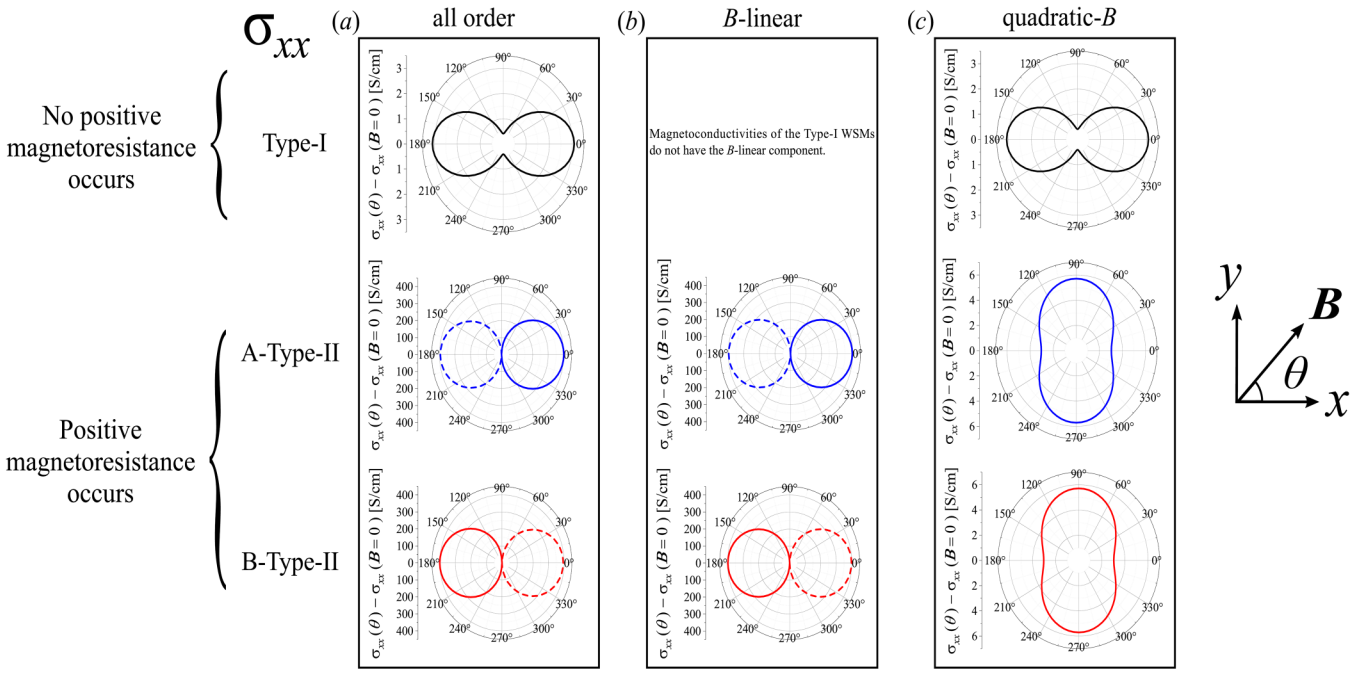

FIG. 4. (a) The longitudinal magnetoconductivities σ_{xx} of type-I WSMs ($\gamma = 0$), A-type-II WSMs ($\gamma = -2.5t$), and B-type-II WSMs ($\gamma = 2.5t$). (b) and (c) The B-linear components and the quadratic-B components of longitudinal magnetoconductivities, respectively. The magnetic field of $\boldsymbol{B} = (3\cos\theta, 3\sin\theta, 0)$ T is applied in the xy-plane, where θ is the angle between the x-axis and the magnetic field. The black, blue, and red lines show the longitudinal magnetoconductivities of type-I, A-type-II, and B-type-II WSMs, respectively. The solid curves represent the positive values, and the dotted curves represent the negative values.

x-axis, on the other hand, the electron carrier at the left Weyl cone sinks into the bulk to the negative direction of the x-axis. As a result, the chiral chemical potential of the left Weyl cone is lower than that of the right Weyl cone. Therefore, we find that the chiral anomaly causes the opposite phenomenon depending on whether the WSMs have the electron-like zeroth Landau energy-levels or the hole-like zeroth Landau energy-levels. The current by the chiral magnetic effect is given as follows:[19,30]

$$\boldsymbol{j}_c = \frac{e^2}{h^2}\Delta\epsilon\boldsymbol{B}, \tag{13}$$

where $\Delta\epsilon$ is the difference between the chiral chemical potentials of the Weyl cone with a chirality of $\chi = +1$ and the Weyl cone with a chirality of $\chi = -1$. Note that in all the cases of type-I, A-type-II, and B-type-II WSMs, the value of chirality at the right Weyl point of $\boldsymbol{k} = (k_0, 0, 0)$ is equal to -1 and that at the left Weyl point of $\boldsymbol{k} = (-k_0, 0, 0)$ is equal to $+1$. The values of $\Delta\epsilon$ of type-I and A-type-II WSMs are positive. However, those of B-type-II WSMs are negative. We find that the signs of the values of $\Delta\epsilon$ are determined by whether these WSMs have the electron-like or the hole-like zeroth Landau energy-levels. From Eq. (13), we find that in both type-I and A-type-II WSMs (in the case of the positive $\Delta\epsilon$), the electric current flows in the same direction as the magnetic field. On the other hand, we find that in B-type-II WSMs (in the case of the negative $\Delta\epsilon$), the electric current flows in the opposite direction to the magnetic field. This is why B-type-II WSMs show the positive longitudinal magnetoresistance with the magnetic field applied in the positive direction of the x-axis. Second, we investigate the longitudinal magnetoconductivities under the magnetic field applied in the negative direction of the x-axis. The values of $\Delta\epsilon$ of A-type-II WSMs are positive with the magnetic field applied in the negative direction of the x-axis since they have the electron-like zeroth Landau energy-levels. On the other hand, those of type-I and B-type-II WSMs are negative since they have the hole-like zeroth Landau energy-levels. As a result, type-I and B-type-II WSMs show the negative longitudinal magnetoresistance. Then, A-type-II WSMs show the positive longitudinal magnetoresistance.

Since A-type-II (B-type-II) WSMs have the electron-like (the hole-like) zeroth Landau energy-levels regardless of the direction of the magnetic field, the values of $\Delta\epsilon$ are positive (negative). As you can see from Eq. (13), in A-type-II (B-type-II) WSMs, the current flows in the same (opposite) direction as (to) the magnetic field. On the other hand, since type-I WSMs have the electron-like (the hole-like) zeroth Landau energy-levels with the magnetic field applied in the positive (the negative) direction of the x-axis, the

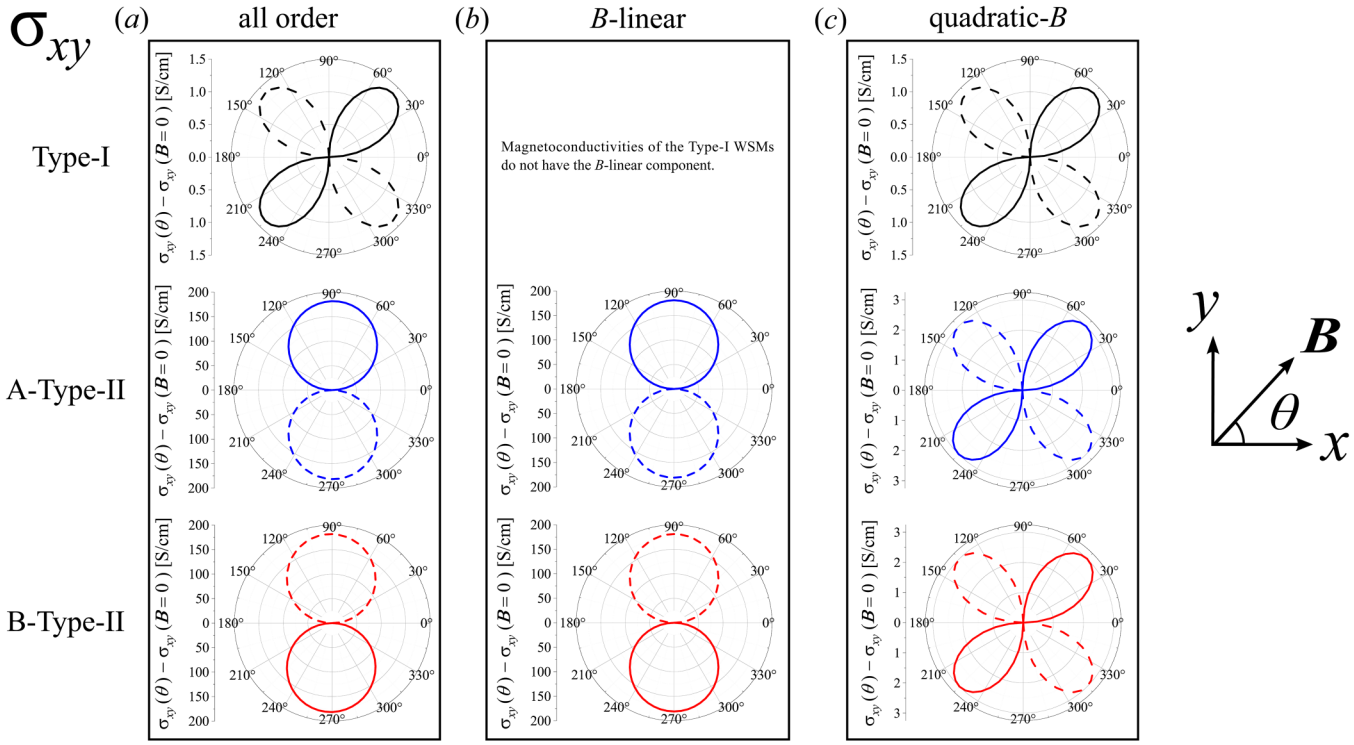

FIG. 5. (a) The transverse magnetoconductivities σ_{xy} of type-I WSMs ($\gamma = 0$), A-type-II WSMs ($\gamma = -2.5t$), and B-type-II WSMs ($\gamma = 2.5t$). (b) and (c) The B-linear components and quadratic-B components of transverse magnetoconductivities, respectively. The magnetic field of $\boldsymbol{B} = (3\cos\theta, 3\sin\theta, 0)$ T is applied in the xy-plane, where θ is the angle between the x-axis and the magnetic field. The black, blue, and red lines show the transverse magnetoconductivities of type-I, A-type-II, and B-type-II WSMs, respectively. The solid curves represent the positive values, and the dotted curves represent the negative values.

values of $\Delta\epsilon$ are positive (negative). Since the signs of the values of $\Delta\epsilon$ are the same as the sign of the magnetic field, these signs cancel each other in Eq. (13). As a result, type-I WSMs show the negative longitudinal magnetoresistance regardless of the direction of the magnetic field. In addition to these type-I and type-II WSMs, there also exist type-III WSMs[31–33] lying at the transition between type-I and type-II WSMs. The model Hamiltonian that we utilize in this study can become type-III WSMs when we set the parameters $t_x = t$, $t' = m = 2t$, and $\gamma = \pm 2t$. These type-III WSMs also show the positive longitudinal magnetoresistance.

Moreover, Figs. 4(b) and 4(c) show B-linear components and quadratic-B components of the longitudinal magnetoconductivities, respectively. In this study, we can ignore the third and higher order components of the magnetic field B since they are estimated to be very small. The longitudinal magnetoconductivities of type-I WSMs have only the quadratic-B components as shown in Fig. 4(c). The longitudinal magnetoconductivities of type-I WSMs show the $\cos^2\theta$ dependence resulting in the anisotropic magnetoresistance (AMR). This angle-dependence originates from the fact that the magnetoconductivity is proportional to the square of the magnetic field parallel with an electric field. Note that an electric field is applied along the x-direction in this calculation. Then, the magnetic field parallel with an electric field is $3\cos\theta$ T. It is experimentally observed that the AMR of Cd_3As_2[34] and Na_3Bi[35] behaves as the square of the magnetic field parallel with an electric field. On the other hand, the longitudinal magnetoconductivities of A-type-II and B-type-II WSMs have both of the B-linear and quadratic-B components as shown in Figs. 4(b) and 4(c). We find that the B-linear components are dominant.

These origins can be explained by the Onsager reciprocity relations. The original Hamiltonian of Eq. (1) does not have TRS. However, in this study, we perform the numerical calculations in the low-energy region. In the low-energy region, we can transform Eq. (1) into the following Hamiltonian:

$$H(k_x \pm k_0, k_y, k_z) = \mp(2t\sin k_0)k_x\sigma_x - 2tk_y\sigma_y - 2tk_z\sigma_z \mp (\gamma \sin k_0)k_x\sigma_0. \quad (14)$$

When γ is equal to zero, the TRS recovers in the above Hamiltonian. According to the Onsager reciprocity relations $\sigma_{ij}(\boldsymbol{B}) = \sigma_{ji}(-\boldsymbol{B})$, the B-linear component of magnetoconductivity is forbidden when TRS holds. Note that the Onsager reciprocity relations hold only when the system is time reversal invariant. As a result, the magnetoconductivities of type-I WSMs ($\gamma = 0$) do not have B-linear components. On the other hand, those of type-II WSMs ($\gamma \neq 0$) have B-linear components.

Therefore, the longitudinal magnetoconductivities of A-type-II and B-type-II WSMs behave as $\cos\theta$ and $-\cos\theta$,[36] respectively. Depending on whether the positive or negative

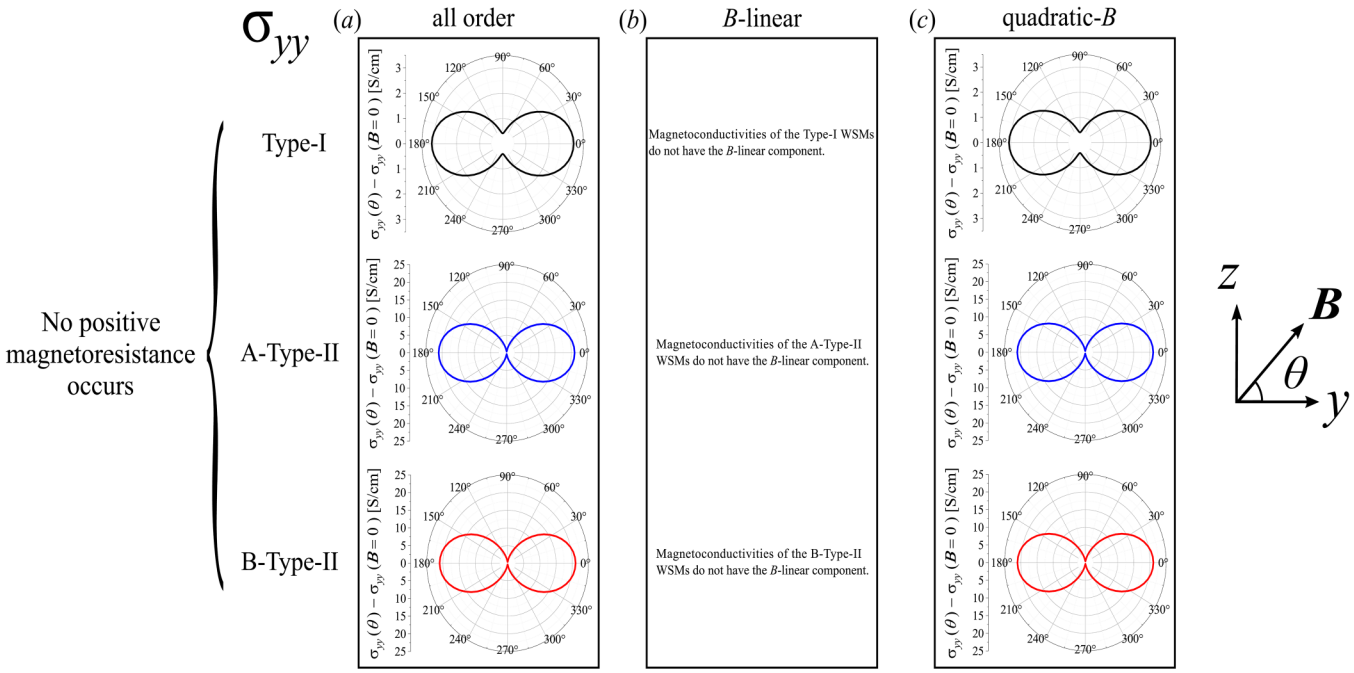

FIG. 6. (a) The longitudinal magnetoconductivities σ_{yy} of type-I WSMs ($\gamma = 0$), A-type-II WSMs ($\gamma = -2.5t$), and B-type-II WSMs ($\gamma = 2.5t$). (b) and (c) The B-linear components and the quadratic-B components of longitudinal magnetoconductivities, respectively. The magnetic field of $\boldsymbol{B} = (0, 3\cos\theta, 3\sin\theta)$ T is applied in the yz-plane, where θ is the angle between the x-axis and the magnetic field. The black, blue, and red lines show the longitudinal magnetoconductivities of type-I, A-type-II, and B-type-II WSMs, respectively.

longitudinal magnetoresistance occurs, the sign of the dependence of $\cos\theta$ of longitudinal magnetoconductivity changes.

Figure 5 shows the transverse magnetoconductivities σ_{xy} under the magnetic field of $\boldsymbol{B} = (3\cos\theta, 3\sin\theta, 0)$ T in the xy-plane. At first sight, we find that the transverse magnetoconductivities of type-I WSMs do not have B-linear components of them. Next, we find that the quadratic-B components of transverse magnetoconductivities of type-I WSMs show the $\sin 2\theta$ dependence leading to the planar Hall effect. It is well known that the planar Hall effect is caused by a difference between the conductivity parallel with the magnetic field and that perpendicular to the magnetic field. The difference between the conductivities is considered to originate from the negative longitudinal magnetoresistance. Specifically, the σ_{xx} is enhanced by the negative longitudinal magnetoresistance. Thus, the difference between the conductivities arises. As a result, the transverse magnetoconductivities of type-I WSMs show the planar Hall effect according to the equation in the reference.[37] On the other hand, the transverse magnetoconductivities of A-type-II and B-type-II WSMs have the B-linear components as shown in Fig. 5(b). We find that the B-linear components are dominant in type-II WSMs. As a result, the transverse magnetoconductivities of A-type-II (B-type-II) WSMs behave as $\sin\theta$ ($-\sin\theta$). The transverse magnetoconductivities of A-type-II (B-type-II) WSMs decrease when the magnetic field is applied in the negative (the positive) direction of the y-axis. However, in the transverse magnetoconductivities, the decrease of the magnetoconductivities is a part of the planar Hall effect, which does not mean the positive longitudinal magnetoresistance.

Next, we investigate whether or not longitudinal magnetoresistances show the positive values when both the electric and magnetic fields are applied perpendicular to the direction of Weyl point separation (i.e., in the yz-plane). Figure 6 shows the longitudinal magnetoconductivities σ_{yy} under the magnetic field of $\boldsymbol{B} = (0, 3\cos\theta, 3\sin\theta)$ T in the yz-plane. Here, θ is the angle between the y-axis and the external magnetic field. At first sight, we find that all the longitudinal magnetoconductivities of type-I, A-type-II, and B-type-II WSMs do not have B-linear components of them. Next, it is found that the longitudinal magnetoconductivities of type-I, A-type-II, and B-type-II WSMs increase as the direction of the magnetic field becomes more aligned to that of the electric field, regardless of the inclination of Weyl cone γ. Moreover, these magnetoconductivities behave like the AMR. Like the cases of the longitudinal magnetoconductivities σ_{xx}, we can explain the numerical results in Fig. 6 utilizing Eq. (13). First, we consider the case where both the electric and the magnetic field are applied in the positive direction of the y-axis. The electron carrier

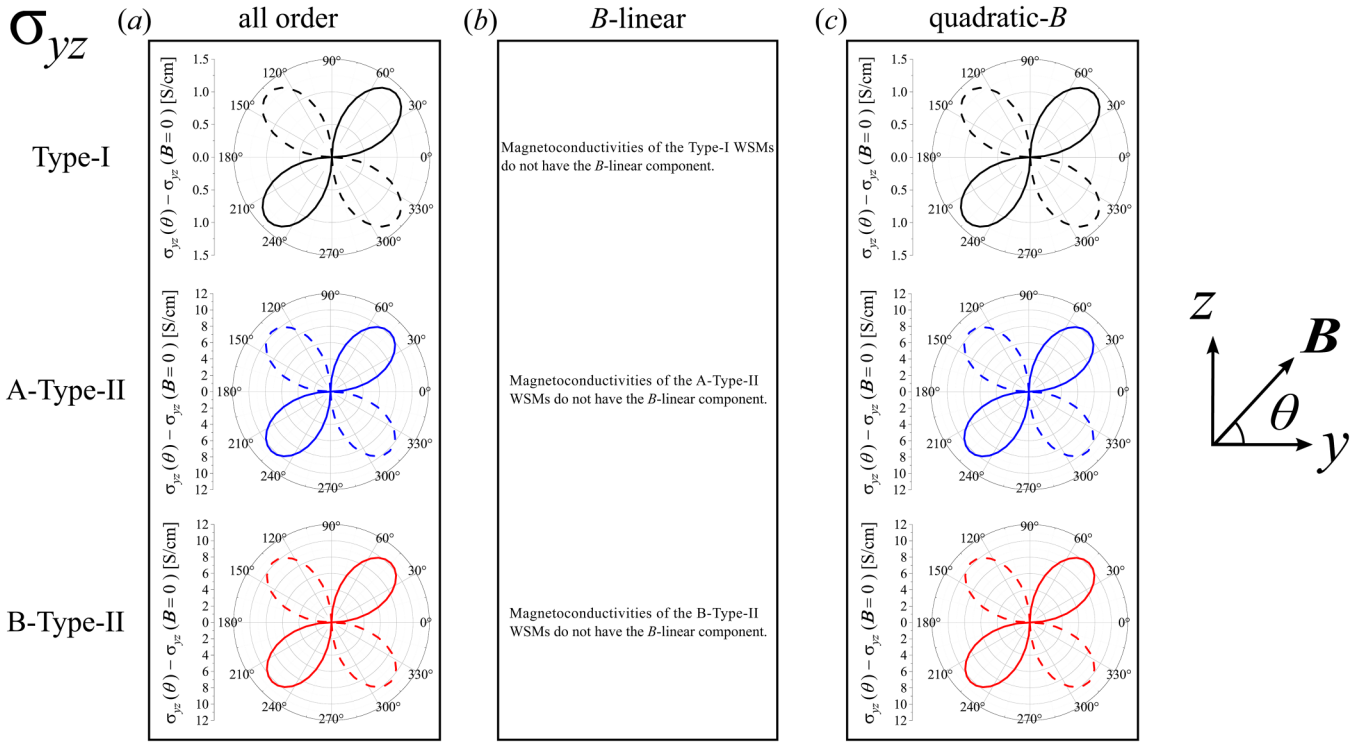

FIG. 7. (a) The transverse magnetoconductivities σ_{yz} of type-I WSMs ($\gamma = 0$), A-type-II WSMs ($\gamma = -2.5t$), and B-type-II WSMs ($\gamma = 2.5t$). (b) and (c) The B-linear components and the quadratic-B components of transverse magnetoconductivities, respectively. The magnetic field of $\boldsymbol{B} = (0, 3\cos\theta, 3\sin\theta)$ T is applied in the yz-plane, where θ is the angle between the x-axis and the magnetic field. The black, the blue, and red lines show the transverse magnetoconductivities of type-I, A-type-II, and B-type-II WSMs, respectively. The solid curves represent the positive values and the dotted curves represent the negative values.

at Weyl cone having $\chi = +1$ moves up from the bulk to the negative direction of the y-axis; on the other hand, the electron carrier at the Weyl cone having $\chi = -1$ sinks into the bulk to the negative direction of the y-axis. As a result, the values of $\Delta\epsilon$ are positive since the chiral chemical potential of the Weyl cone having $\chi = +1$ ($\chi = -1$) increases (decreases). From Eq. (13), we find that in all the cases of type-I, A-type-II, and B-type-II WSMs, the magnetoconductivities increase since the electric current by the chiral magnetic effect flows in the positive direction of the y-axis. Next, we consider the case where the electric field is applied in the positive direction of the y-axis and the magnetic field is applied in the negative direction of that. The electron carrier at the Weyl cone having $\chi = +1$ sinks into the bulk to the negative direction of the y-axis, on the other hand, the electron carrier at the Weyl cone having $\chi = -1$ moves up from the bulk to the negative direction of the y-axis. As a result, the values of $\Delta\epsilon$ are negative. The electric current by the chiral magnetic effect flows in the positive direction of the y-axis since the signs of both the values of $\Delta\epsilon$ and the magnetic field cancel each other in Eq. (13). Therefore, we find that in all the cases of type-I, A-type-II, and B-type-II WSMs, the longitudinal magnetoconductivities increase when the magnetic field is applied in both the positive and negative direction of the y-axis.

Next, we investigate how the transverse magnetoconductivities σ_{yz} behave when the longitudinal magnetoconductivities of type-I, A-type-II, and B-type-II WSMs show only the positive values. Figure 7 shows the transverse magnetoconductivities σ_{yz} under the magnetic field of $\boldsymbol{B} = (0, 3\cos\theta, 3\sin\theta)$ T in the yz-plane. At first sight, as with the longitudinal magnetoconductivities σ_{yy}, we find

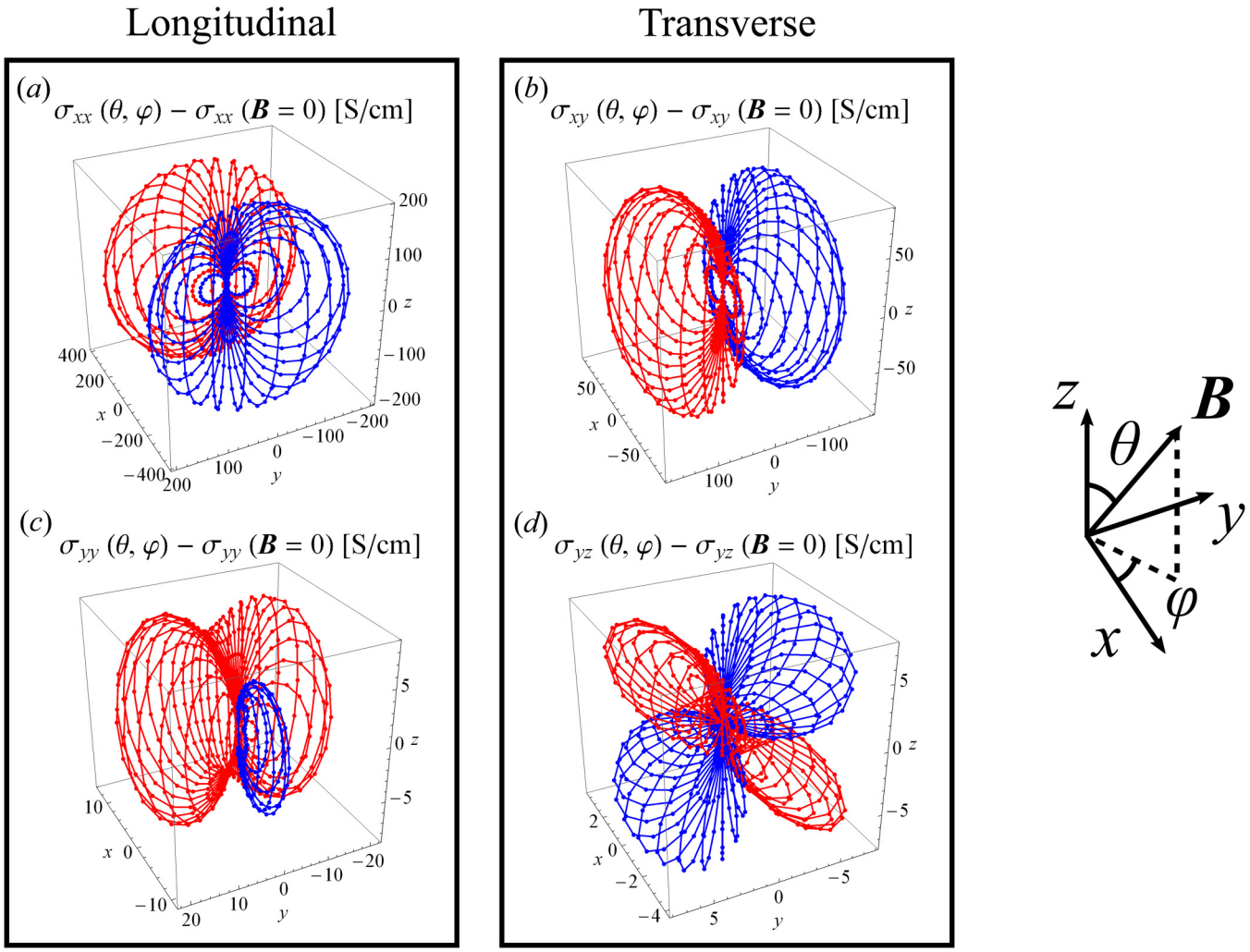

FIG. 8. The three-dimensional wire-frame plots of the magnetoconductivities (*a*) σ_{xx}, (*b*) σ_{xy}, (*c*) σ_{yy}, and (*d*) σ_{yz} of the A-type-II WSMs. The magnetic field of $\boldsymbol{B} = (3\sin\theta\cos\varphi, 3\sin\theta\sin\varphi, 3\cos\theta)$ T is applied, where θ is the angle between the z-axis and the external magnetic field and φ is the angle between the x-axis and the projected component of the external magnetic field on the xy-plane. The red curves show the positive values, and the blue curves show the negative values.

that all the transverse magnetoconductivities of type-I, A-type-II, and B-type-II WSMs do not have B-linear components of them. Next, it is found that the transverse magnetoconductivities of type-I, A-type-II, and B-type-II WSMs behave like the planar Hall effect, regardless of the inclination of Weyl cone γ. Furthermore, we have discovered that the direction of the inclination of the Weyl cone is largely related to the existence of the B-linear component of magnetoconductivity. Note that in this study, Weyl cone is tilted in the k_x-direction. The magnetoconductivities σ_{xx} and σ_{xy} have the B-linear components. On the other hand, the magnetoconductivities σ_{yy} and σ_{yz} do not have the B-linear component. Only the magnetoconductivity in the direction where the Weyl cone is tilted has the B-linear component.

Finally, we show the three-dimensional wire-frame plots of the magnetoconductivities of the A-type-II WSMs under the magnetic field of $\boldsymbol{B} = (3\sin\theta\cos\varphi, 3\sin\theta\sin\varphi, 3\cos\theta)$ T in Fig. 8. Here, θ is the angle between the z-axis and the external magnetic field and φ is the angle between the x-axis and the projected component of the external magnetic field on the xy-plane. The red curves show the positive values, and the blue curves show the negative values. This 3D wire-frame plots allow us to understand the behavior of magnetoconductivities by the direction of the magnetic field at a glance.

IV. CONCLUSION

In this study, we have elucidated the origin of the positive longitudinal magnetoresistance. The A-type-II WSMs under the magnetic field applied in the negative direction of the x-axis and the B-type-II WSMs under the magnetic field applied in the positive direction of the x-axis show the positive longitudinal magnetoresistance as shown in Fig. 4(a). The positive longitudinal magnetoresistance occurs under the following three conditions:

- The TRS has to be broken due to the inclination of the Weyl cone. When the TRS is broken, the magnetoconductivity can have the B-linear component, which is usually forbidden by the Onsager reciprocity relations.
- The electric field has to be applied in the direction where Weyl points are separated. Note that in this study, we have applied the electric field in the direction where the Weyl point with a chirality of $\chi = +1$ is the starting point and the Weyl point with a chirality of $\chi = -1$ is the end point.
- The magnetic field has to be applied "in the opposite direction to the electric field" or "the same direction as the electric field" depending on whether the WSMs have "the electron-like" or "the hole-like" zeroth Landau energy-levels. If the WSMs have the electron-like zeroth Landau energy-levels under the magnetic field applied in the opposite direction to the electric field like A-type-II WSMs, the electron carrier moves in the opposite direction to the electric field. The difference between the chiral chemical potentials of the left Weyl cone with $\chi = +1$ and the right Weyl cone with $\chi = -1$ becomes a positive value. As a result, the current by the chiral magnetic effect flows in the same direction as the magnetic field. When the magnetic field is applied in the opposite direction to the electric field, the positive longitudinal magnetoresistance occurs in the above situation. On the other hand, if the WSMs have the hole-like zeroth Landau energy-levels under the magnetic field applied in the same direction as the electric field like B-type-II WSMs, the hole carrier moves in the same direction as the electric field. The difference between the chiral chemical potentials of the left Weyl cone with $\chi = +1$ and the right Weyl cone with $\chi = -1$ becomes a negative value. As a result, the current by the chiral magnetic effect flows in the opposite direction to the magnetic field. When the magnetic field is applied in the same direction as the electric field, the positive longitudinal magnetoresistance occurs in the above situation. From these above results, we can conclude that not only the negative longitudinal magnetoresistance but also the positive longitudinal magnetoresistance can occur due to chiral anomaly in WSMs. Moreover, it is implied that we can make a high MR-ratio device using WSMs if it is possible to tune the inclination of the Weyl cone by the application of the electric field and so on.

ACKNOWLEDGMENTS

This work was partially supported by the JSPS Grants-in-Aid for Scientific Research (Grant Nos. JP16K04872 and JP17H03225), the Center for Spintronics Research Network (CSRN) Tohoku University, and the Dynamic Alliance for Open Innovation Bridging Human, Environment and Materials.

DATA AVAILABILITY

The data that support the findings of this study are available from the corresponding author upon reasonable request.

REFERENCES

[1]C. L. Kane and E. J. Mele, Phys. Rev. Lett. **95**, 146802 (2005).
[2]Z. C. Gu and X. G. Wen, Phys. Rev. B **80**, 155131 (2009).
[3]K. Kondo and R. Ito, J. Phys. Commun. **3**, 055007 (2019).
[4]S. Yuasa, T. Nagahama, A. Fukushima, Y. Suzuki, and K. Ando, Nat. Mater. **3**, 868 (2004).
[5]J. Nitta, T. Akazaki, H. Takayanagi, and T. Enoki, Phys. Rev. Lett. **78**, 1335 (1997).
[6]K. Kondo, J. Appl. Phys. **115**, 17C701 (2014).
[7]Y. Ishida and K. Kondo, J. Magn. Magn. Mater. **493**, 165687 (2020).
[8]Y. Xu, F. Zhang, and C. Zhang, Phys. Rev. Lett. **115**, 265304 (2015).
[9]H. Nielsen and M. Ninomiya, Phys. Lett. B **130**, 389 (1983).
[10]B. Q. Lv, H. M. Weng, B. B. Fu, X. P. Wang, H. Miao, J. Ma, P. Richard, X. C. Huang, L. X. Zhao, G. F. Chen, Z. Fang, X. Dai, T. Qian, and H. Ding, Phys. Rev. X **5**, 031013 (2015).
[11]S. Y. Xu, I. Belopolski, D. S. Sanchez, C. Zhang, G. Chang, C. Guo, G. Bian, Z. Yuan, H. Lu, T. R. Chang, P. P. Shibayev, M. L. Prokopovych, N. Alidoust, H. Zheng, C. C. Lee, S. M. Huang, R. Sankar, F. Chou, C. H. Hsu, H. T. Jeng, A. Bansil, T. Neupert, V. N. Strocov, H. Lin, S. Jia, and M. Z. Hasan, Sci. Adv. **1**, e150192 (2015).
[12]S. Y. Xu, N. Alidoust, I. Belopolski, Z. Yuan, G. Bian, T. R. Chang, H. Zheng, V. N. Strocov, D. S. Sanchez, G. Chang, C. Zhang, D. Mou, Y. Wu, L. Huang, C. C. Lee, S. M. Huang, B. Wang, A. Bansil, H. T. Jeng, T. Neupert, A. Kaminski, H. Lin, S. Jia, and M. Zahid Hasan, Nat. Phys. **11**, 748 (2015).
[13]Sudesh, P. Kumar, P. Neha, T. Das, and S. Patnaik, Sci. Rep. **7**, 46062 (2017).
[14]A. C. Niemann, J. Gooth, S. C. Wu, S. Bäßler, P. Sergelius, R. Hühne, B. Rellinghaus, C. Shekhar, V. Süß, M. Schmidt, C. Felser, B. Yan, and K. Nielsch, Sci. Rep. **7**, 43394 (2017).

[15]P. Li, Y. Wen, X. He, Q. Zhang, C. Xia, Z. M. Yu, S. A. Yang, Z. Zhu, H. N. Alshareef, and X. X. Zhang, Nat. Commun. **8**, 2150 (2017).
[16]J. Jiang, Z. K. Liu, Y. Sun, H. F. Yang, C. R. Rajamathi, Y. P. Qi, L. X. Yang, C. Chen, H. Peng, C. C. Hwang, S. Z. Sun, S. K. Mo, I. Vobornik, J. Fujii, S. S. P. Parkin, C. Felser, B. H. Yan, and Y. L. Chen, Nat. Commun. **8**, 13973 (2017).
[17]A. Pal, M. Chinotti, L. Degiorgi, W. Ren, and C. Petrovic, Physica B **536**, 64 (2018).
[18]A. A. Burkov, J. Phys.: Condens. Matter **27**, 113201 (2015).
[19]Q. Li and D. E. Kharzeev, Nucl. Phys. A **956**, 107 (2016).
[20]J. Hu, J. Y. Liu, D. Graf, S. M. A. Radmanesh, D. J. Adams, A. Chuang, Y. Wang, I. Chiorescu, J. Wei, L. Spinu, and Z. Q. Mao, Sci. Rep. **6**, 18674 (2016).
[21]F. Arnold, C. Shekhar, S. C. Wu, Y. Sun, R. D. dos Reis, N. Kumar, M. Naumann, M. O. Ajeesh, M. Schmidt, A. G. Grushin, J. H. Bardarson, M. Baenitz, D. Sokolov, H. Borrmann, M. Nicklas, C. Felser, E. Hassinger, and B. Yan, Nat. Commun. **7**, 11615 (2016).
[22]N. Kumar, S. N. Guin, C. Felser, and C. Shekhar, Phys. Rev. B **98**, 041103 (2018).
[23]J. Yang, W. L. Zhen, D. D. Liang, Y. J. Wang, X. Yan, S. R. Weng, J. R. Wang, W. Tong, L. Pi, W. K. Zhu, and C. J. Zhang, Phys. Rev. Mater. **3**, 014201 (2019).
[24]T. M. McCormick, I. Kimchi, and N. Trivedi, Phys. Rev. B **95**, 075133 (2017).
[25]S. Q. Shen, M. Ma, X. C. Xie, and F. C. Zhang, Phys. Rev. Lett. **92**, 256603 (2004).
[26]S. Q. Shen, Y. J. Bao, M. Ma, X. C. Xie, and F. C. Zhang, Phys. Rev. B **71**, 155316 (2005).
[27]D. T. Son and B. Z. Spivak, Phys. Rev. B **88**, 104412 (2013).
[28]K. Das and A. Agarwal, Phys. Rev. B **99**, 085405 (2019).
[29]A. Kundu, Z. B. Siu, H. Yang, and M. B. A. Jalil, New J. Phys. **22**, 083081 (2020).
[30]N. P. Armitage, E. J. Mele, and A. Vishwanath, Rev. Mod. Phys. **90**, 015001 (2018).
[31]G. E. Volovik, JETP Lett. **104**, 645 (2016).
[32]H. Huang, K. H. Jin, and F. Liu, Phys. Rev. B **98**, 121110 (2018).
[33]S. M. Rafi-Ul-Islam, Z. Bin Siu, and M. B. A. Jalil, Commun. Phys. **3**, 72 (2020).
[34]H. Li, H. He, H. Z. Lu, H. Zhang, H. Liu, R. Ma, Z. Fan, S. Q. Shen, and J. Wang, Nat. Commun. **7**, 10301 (2016).
[35]J. Xiong, S. K. Kushwaha, T. Liang, J. W. Krizan, M. Hirschberger, W. Wang, R. J. Cava, and N. P. Ong, Science **350**, 413 (2015).
[36]S. Nandy, G. Sharma, A. Taraphder, and S. Tewari, Phys. Rev. Lett. **119**, 176804 (2017).
[37]J. P. Jan, Solid State Phys. **5**, 1 (1957).